Eur. Phys. J. A **7**, 507–518 (2000)

THE EUROPEAN PHYSICAL JOURNAL A

$(p, \pi^{\pm})$ correlations in central heavy-ion collisions at $1 \div 2$ AGeV*

A.B. Larionov[a], W. Cassing, M. Effenberger, U. Mosel

Institut für Theoretische Physik, Universität Giessen, 35392 Giessen, Germany

Received: 18 October 1999 / Revised version: 4 February 2000
Communicated by W. Weise

Abstract. The proton – charged pion correlated emission is studied in the reactions Au (1.06 AGeV) + Au, Ni (1.06 and 1.93 AGeV) + Ni and Ni (1.97 AGeV) + Cu within the BUU approach. The associated invariant mass distributions are shifted to smaller energies with respect to the free $\Delta(1232)$ mass distribution due to kinematical reasons. We find that the existing and partly conflicting experimental data do not allow to draw definite conclusions on the in-medium modification of the $\Delta(1232)$.

PACS. 25.75.-q Relativistic heavy-ion collisions – 25.75.Dw Particle and resonance production – 25.75.Gz Particle correlations

1 Introduction

The properties of the baryon resonances in hot and dense nuclear matter are the subject of recent theoretical [1–5] and experimental [6–8] studies. The most important question is, how the centroid energies and the widths of the resonances are modified in nuclear matter.

In [6] the invariant mass spectra of correlated $(p, \pi^{\pm})$ pairs were measured in collisions of Ni+Cu at 1.97 AGeV. It is demonstrated in [6], that the peaks of the spectra are shifted to smaller invariant masses by about -50 MeV with respect to the free Δ mass; this shift increases with the collision centrality. Furthermore, in [7,8] the mass distributions of the baryon resonances excited in Au+Au and Ni+Ni central collisions at energies between 1 and 2 AGeV were deduced experimentally on the basis of two methods: (i) by defolding the p_t spectra of charged pions, and (ii) from invariant masses of $(p, \pi^{\pm})$ pairs. The peaks of the Δ-mass distributions extracted in [7] are shifted on average by -83 MeV for Au+Au and -63 MeV for Ni+Ni collisions with respect to the free Δ-resonance[1].

In this work we have performed BUU transport calculations (see [4,9] for a general review and [10] for the description of the latest version of the BUU model) for collisions of Au+Au at 1.06 AGeV, Ni+Ni at 1.06 and 1.93 AGeV and Ni+Cu at 1.97 AGeV in order to study the invariant mass spectrum of correlated $(p, \pi^{\pm})$ pairs produced by resonance decay. The aim of this work is twofold: (i) to study the mechanism of the correlated pair emission, and (ii) by comparison with the experimental data try to get information on the in-medium modification of the Δ-resonance.

The structure of this paper is as follows: In Sect. 2 the space-time picture of the correlated $(p, \pi^{\pm})$ pair emission is studied. In Sect. 3 the final correlated $(p, \pi^{\pm})$ invariant mass spectra are presented and compared to thermodynamic model predictions. The possibility to extract these spectra within the mixed event technique [11] is demonstrated and a comparison to the experimental data of [6–8] is performed. A summary and conclusions are given in Sect. 4.

2 Space-time picture of the correlated $(p, \pi^{\pm})$ pair emission

All calculations performed in this work involve the BUU model of [10], including a momentum-dependent mean field with a compressibility modulus $K = 280$ MeV as well as vacuum spectral functions for all resonances. We shall call this parameterset as "standard" below for brevity. Modifications of spectral functions will be discussed explicitly. Here we only briefly describe the most important physical inputs of the BUU model (see [10] for details).

The mechanism of pion production implemented in the BUU model includes two steps (besides a small contribution from direct $NN \to NN\pi$ processes): In the first step the $\Delta(1232)$ and higher baryon resonances are excited in inelastic nucleon-nucleon collisions: $NN \to NR$, where N

* Supported by BMBF and GSI Darmstadt

[a] On leave from RRC "I.V. Kurchatov Institute", 123182 Moscow, Russia

[1] The mass shifts reported in [7] are given relative to the free Δ peak of 1.210 GeV, which arises from the $\mathcal{B}$-function of [5] (see also dashed line in Fig. 14). In our work, the mass distribution of the free Δ resonance is peaked at 1.224 GeV (see solid line in Fig. 14) and we discuss all mass shifts with respect to this value.

stands for a nucleon and R for a resonance. At a collision energy $1 \div 2$ AGeV dominantly the $NN \to N\Delta(1232)$ channel determines the inelastic part of the total nucleon-nucleon cross section. The masses of the produced resonances are chosen according to their vacuum spectral functions

$$\mathcal{A}(M) = \frac{2}{\pi} \frac{M^2 \Gamma(M)}{(M^2 - M_{\rm pole}^2)^2 + M^2 \Gamma^2(M)} \ , \qquad (1)$$

where $M_{\rm pole}$ is the pole mass and $\Gamma(M)$ is the total mass-dependent decay width. In the particular case of the Δ-resonance $M_{\rm pole} = M_\Delta = 1.232$ GeV, while

$$\Gamma(M) = \Gamma_\Delta \left(\frac{q}{q_r} \right)^3 \frac{M_\Delta}{M} \frac{\beta_r^2 + q_r^2}{\beta_r^2 + q^2} \qquad (2)$$

is the free space mass-dependent Δ-width with $\Gamma_\Delta = 0.118$ GeV, $\beta_r = 0.2$ GeV; q is the pion momentum in the rest frame of the Δ and q_r is the value of q at $M = M_\Delta$.

In the second step the resonance decays into a pion and a nucleon: $R \to \pi N$. The resonance decay at a given time step is simulated by Monte-Carlo using the free space mass-dependent decay width $\Gamma(M)$. The Pauli blocking for the outgoing nucleon is taken into account in our calculations (c.f. [12]). The life time of the Δ-resonance at its pole mass with respect to the pion emission is, therefore, $\tau_{\Delta \to \pi N} = 1/\Gamma_{\Delta \to \pi N} \sim 2$ fm/c, where $\Gamma_{\Delta \to \pi N}$ is the in-medium decay width of the Δ-resonance, which is less than $\Gamma(M)$ due to Pauli blocking [13]. Furthermore, the produced pion can be reabsorbed: $\pi N \to \Delta$. Since the average life time of the Δ is much less than the characteristic time (~ 40 fm/c) of a central heavy-ion collision at $1 \div 2$ AGeV and the pion mean-free-path is quite small ($\lambda_\pi \sim 1$ fm), a chain of processes $\Delta_1 \to \pi_1 N_1$, $\pi_1 N_2 \to \Delta_2$, $\Delta_2 \to \pi_3 N_3$, ... develops. Moreover, the pion and nucleon rescattering on nucleons strongly reduces the probability for the decayed Δ to be "visible". Therefore, only a very small part of Δ-resonances excited in the nucleus-nucleus collision, which is not absorbed in the process $\Delta N \to NN$, can be observed by looking at their decay products – i.e. correlated (π, N) pairs. We define a proton-pion pair as being correlated, if this pair originates from the same resonance and both the proton and the neutron don't rescatter anymore. In other words, we will always consider only *observable* correlated pairs. For the collisions under study we have obtained numerically on average $1 \div 4$ (p, π^-) and $2 \div 6$ (p, π^+) correlated pairs per event in a calculation without acceptance cut (Table 1). After filtering through the central drift chamber (CDC) acceptance of the FOPI Collaboration (for Au+Au and Ni+Ni reactions) the number of correlated pairs decreases by a factor of $3 \div 4$. The CDC acceptance (see [7,14]) was simulated by selecting only particles in the interval $32^o < \Theta_{lab} < 150^o$ and, for π^+, additionally the cut $p_{lab} < 0.65$ GeV/c was applied. In Table 1 we present the numbers $N^{corr}_{(p,\pi^-)}$ and $N^{corr}_{(p,\pi^+)}$ of correlated (p, π^-) and (p, π^+) pairs and corresponding ratios $r^{\pm} = N^{corr}_{(p,\pi^{\pm})}/N^{ran}_{(p,\pi^{\pm})}$. Here $N^{ran}_{(p,\pi^{\pm})}$ is the number of "random" pairs, i.e. those pairs which are composed of a proton and a pion from the same event, but *not* emitted from the same resonance:

$$N^{ran}_{(p,\pi^{\pm})} = N_p N_{\pi^{\pm}} - N^{corr}_{(p,\pi^{\pm})} \ , \qquad (3)$$

where N_p and $N_{\pi^{\pm}}$ are the total numbers of emitted protons and pions, respectively. The ratios $r^{\pm}$ are quite small ($\sim 10^{-3} \div 10^{-2}$) which makes the separation of the true signal from the background (see Sect. 3.2) difficult.

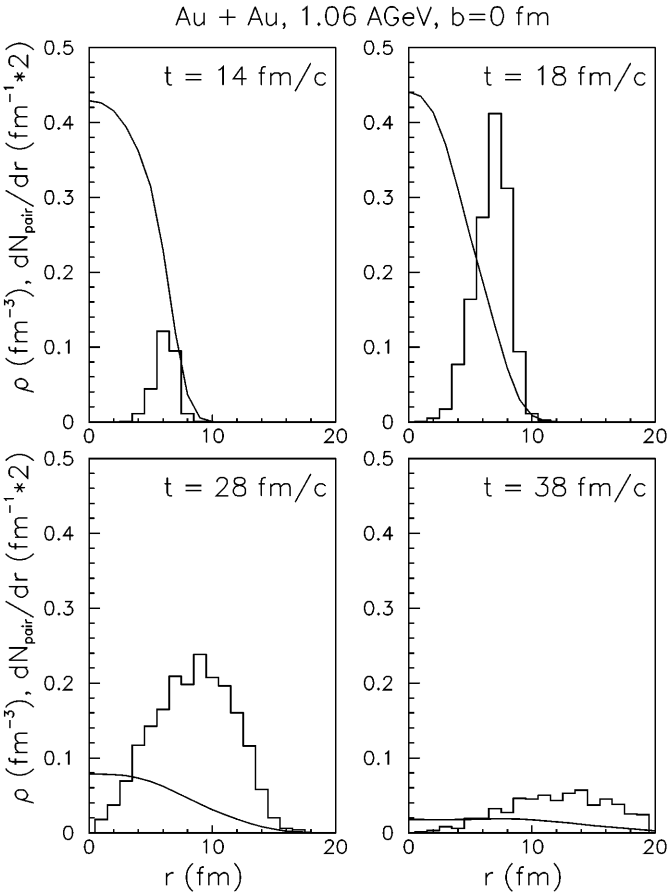

Fig. 1. Radial distributions of the correlated $(p, \pi^{\pm})$ pairs emitted during the time interval $\Delta t = 2$ fm/c (histograms) and the baryon density profiles (solid lines) at various times for a central collision of Au+Au at 1.06 AGeV. Pairs are selected without acceptance cuts

In Fig. 1 we show the time evolution of the nucleon density profile and of the radial distribution of the correlated $(p, \pi^{\pm})$ pairs emitted during the time intervals from $t_i - 1$ fm/c to $t_i + 1$ fm/c, where t_i=14, 18, 28 and 38 fm/c, for the Au+Au system at b=0. Most of the pairs are emitted from the periphery of the system, where the density is low (cf. Fig. 3). We see from Fig. 1, that the intensity of the emission reaches a maximum at $t \simeq 20$ fm/c and then slowly decreases. This is consistent with the pion production rate, which reaches a maximum at t=20 fm/c (cf. Fig. 11 from [15]). Thus, pairs are emitted dominantly at $20 \le t \le 30$ fm/c.

In Fig. 2 the radial dependence of the temperature is presented for a central collision of Au+Au at various

Table 1. Numbers of correlated $(p, \pi^{\pm})$ pairs $N^{corr}_{(p,\pi^{\pm})}$ and ratios of numbers of correlated and random $(p, \pi^{\pm})$ pairs $r^{(\pm)}$ (see text for definitions) for central collisions. In the case of Au+Au and Ni+Ni reactions, the two numbers are given for $N^{corr}_{(p,\pi^{\pm})}$ separated by a comma: before and after filtering through the CDC acceptance. The calculated values of $r^{(\pm)}$ are practically insensitive to the filtering. The experimental values of $r^{(\pm)}$ from [7] are given in brackets. For Ni+Cu collisions all results are unfiltered

System	Energy (AGeV)	$N^{corr}_{(p,\pi^-)}$	$r^{(-)}$ (%)	$N^{corr}_{(p,\pi^+)}$	$r^{(+)}$ (%)
Au+Au	1.06	4.0, 1.2	0.1 (0.6±0.2)	5.7, 2.1	0.3 (0.75±0.25)
Ni+Ni	1.06	1.2, 0.4	0.4 (0.75±0.25)	2.4, 0.7	0.9 (1.0±0.3)
Ni+Ni	1.93	2.5*, 0.6	0.4 (0.6±0.2)	4.9, 1.2	0.9 (1.05±0.3)
Ni+Cu	1.97	2.7*	0.3	4.9	0.7

* including 0.1 (p, π^-) pair due to Λ decays

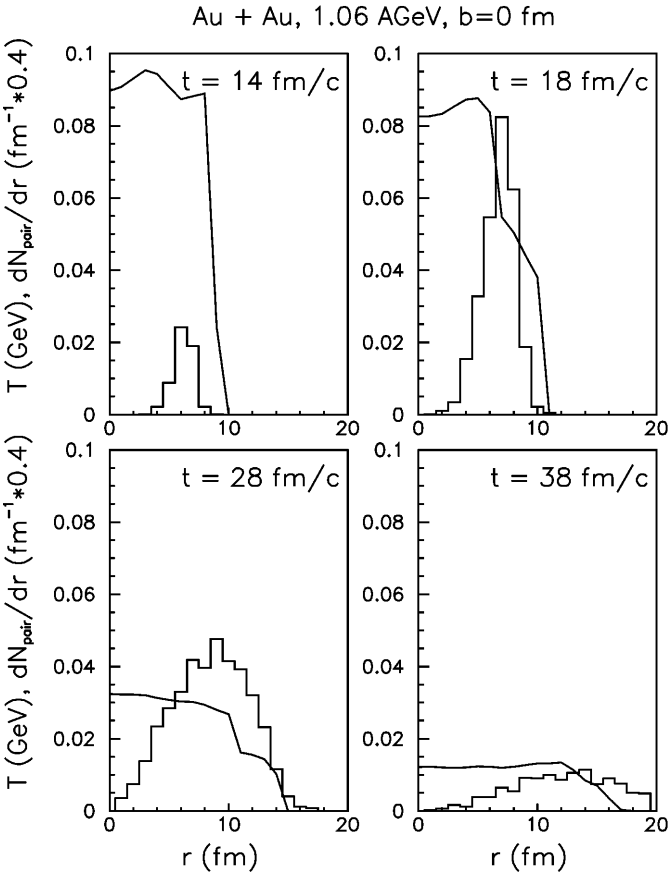

Fig. 2. The same as Fig. 1, but with the kinetic temperature shown by solid lines

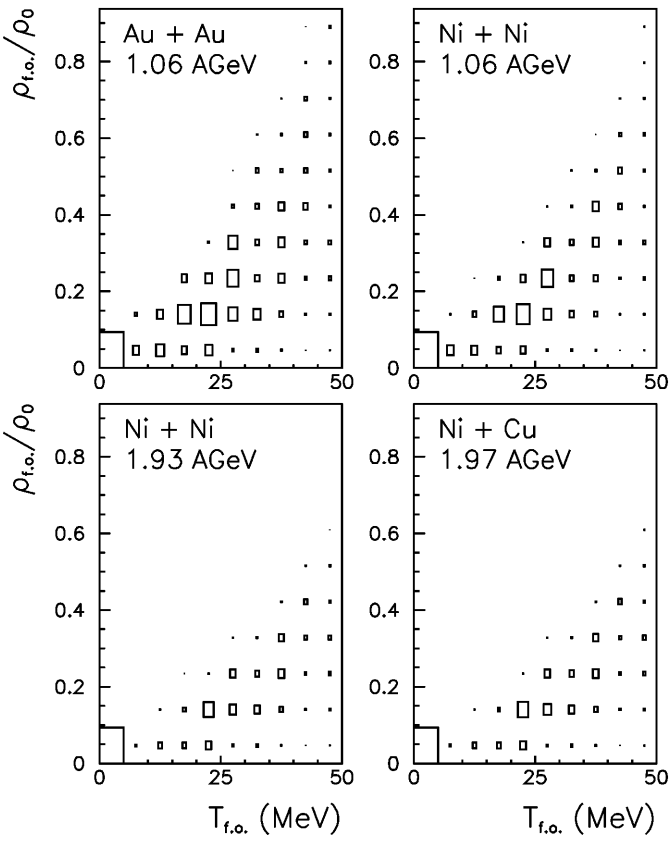

Fig. 3. Freeze-out temperature-density distribution $\partial^2 N_{pair}(T_{f.o.}, \rho_{f.o.})/\partial T_{f.o.} \partial \rho_{f.o.}$ of the correlated (p, π) pairs for central collisions of various systems. The distribution (in a.u.) at a given point $(T_{f.o.}, \rho_{f.o.})$ is proportional to the size of the box. No acceptance cuts were applied

times accompanied by the radial distribution of the correlated $(p, \pi^{\pm})$ pairs. The local temperature was determined on a cubic lattice of 1 fm grid size introduced in the center-of-mass system of the colliding nuclei. A finite temperature Fermi distribution has been adjusted such as to obtain the correct baryon density and average baryon kinetic energy in the local rest frame of the matter element in the lattice cell. During the time period of intensive pair emission, $20 \leq t \leq 30$ fm/c, the temperature at the periphery of the system decreases from 70 MeV to 30 MeV. This implies, that the description of the freeze-out of correlated $(p, \pi^{\pm})$ pairs by some universal value of the temperature is quite schematic. The same conclusion can be obtained with respect to the freeze-out density, which is varying strongly during the period of intensive pair emission (Fig. 1). Nevertheless, one can estimate some average value of the freeze-out density and temperature for a comparison with macroscopic thermodynamic models (cf. [5,16]). Figure 3 shows the distributions of the

Table 2. Mean values and dispersions of the freeze-out density and temperature for central collisions

System	Energy (AGeV)	$\langle\rho_{f.o.}\rangle$ (ρ_0)	σ_ρ (ρ_0)	$\langle T_{f.o.}\rangle$ (MeV)	σ_T (MeV)
Au+Au	1.06	0.41	0.39	39.0	21.0
Ni+Ni	1.06	0.45	0.42	39.4	25.6
Ni+Ni	1.93	0.40	0.42	37.8	24.9
Ni+Cu	1.97	0.41	0.42	37.9	24.9

correlated (p, π) ($\pi = \pi^-, \pi^0, \pi^+$) pairs in the freeze-out temperature-density plane for different reactions. It is interesting that these distributions are very similar for all colliding systems regardless of the system size and, moreover, the collision energy. We always see a doubly peaked structure: at $T_{f.o.} \approx 0$ and $\rho_{f.o.} \approx 0$, that corresponds to the decay of Δ-resonances in vacuum, and at $T_{f.o.} \approx 23$ MeV and $\rho_{f.o.} \approx 0.14\rho_0$, where $\rho_0 = 0.16$ fm^{-3} is the equilibrium nuclear matter density. In Table 2 the mean values and dispersions of the freeze-out parameters are given for all reactions. The distributions are quite broad[2] and the mean values of the freeze-out density and temperature are essentially higher than the maxima of the actual distributions in Fig. 3: $\langle\rho_{f.o.}\rangle \simeq 0.41\rho_0$ and $\langle T_{f.o.}\rangle \simeq 39$ MeV. The baryon chemical potential extracted within the thermal model (see next section) at $\rho_B = 0.41\rho_0$ and $T = 39$ MeV is $\mu_B = 889$ MeV. These freeze-out parameters are different from the thermal model analysis of Cleymans et al. for Au + Au collisions at 1 AGeV [16]: i.e. $T_{f.o.} = 50$ MeV, $\mu_B = 850$ MeV.

3 Invariant mass distributions of correlated $(p, \pi^{\pm})$ pairs

First we discuss the results of the direct analysis of the correlated $(p, \pi^{\pm})$ pairs which can be unambiguously identified in the BUU calculation. In Fig. 4 the invariant mass spectrum of correlated $(p, \pi^{\pm})$ pairs is shown (solid line) for Au+Au central collisions. This spectrum was extracted by stopping the time evolution at $t = 40$ fm/c. All the correlated pairs present in the system at this time plus the pairs produced by the forced decay of resonances were counted. We have checked that stopping the time evolution at later times does not influence the extracted spectrum of the pairs within the accuracy of our statistics, since for Au + Au central collision at 1.06 AGeV only 2% of all baryon-baryon collisions happen after 40 fm/c. In order to understand, how various time intervals are contributing to the total invariant mass spectrum, we show also in Fig. 4 the partial spectra given by the pairs emitted at $t < 20$ fm/c and at $t < 30$ fm/c. We see that, in agreement with the discussion in the previous section, the total spectrum is dominantly composed from pairs emitted in the interval $20 < t < 30$ fm/c and that the low-mass pairs come primarily from very late times.

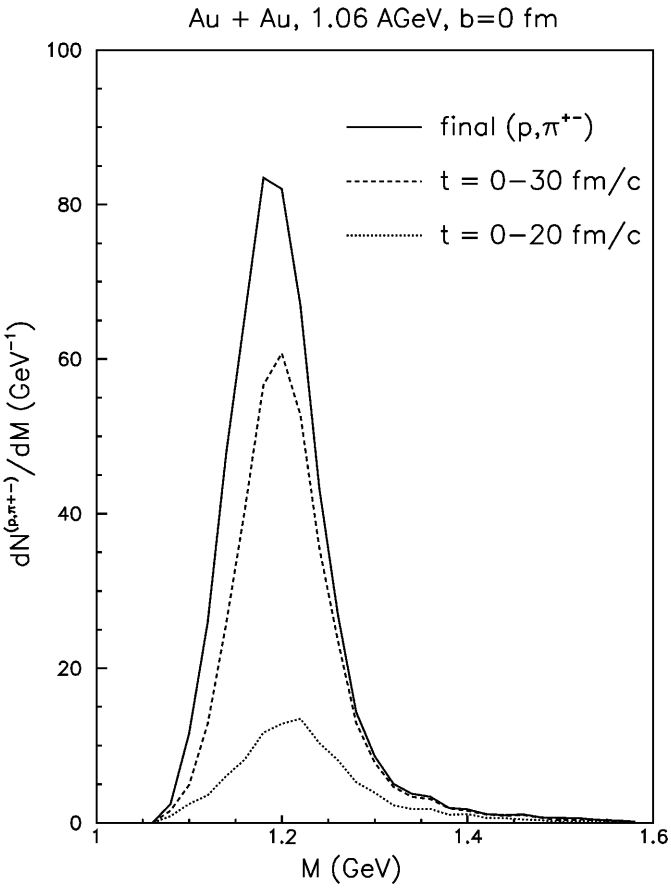

Fig. 4. Invariant mass distribution of the correlated $(p, \pi^{\pm})$ pairs emitted at the time intervals $t = 0 \div 20$ fm/c (dotted line), $t = 0 \div 30$ fm/c (dashed line) and the total spectrum after induced decay of residual Δ's at $t = 40$ fm/c (solid line) for a central collision of Au+Au at 1.06 AGeV. No acceptance cuts were applied

3.1 Analysis within the thermodynamical model

We have analysed the final spectra of correlated $(p, \pi^{\pm})$ pairs using a simple thermodynamical model including nucleons, $\Delta(1232)$ resonances and free pions. For a given temperature T and baryon density ρ_B the baryon chemical potential μ_B can be exctracted from the equation:

$$\rho_B = \rho_N + \rho_\Delta \ , \tag{4}$$

where ρ_N and ρ_Δ are the densities of nucleons and deltas:

$$\rho_N = 4 \int \frac{d^3p}{(2\pi\hbar)^3} \frac{1}{\exp\left(\epsilon_p - \mu_B\right)/T + 1} \ , \tag{5}$$

$$\rho_\Delta = 16 \int\limits_{M_N+M_\pi}^{\infty} dM \mathcal{A}(M) \int \frac{d^3p}{(2\pi\hbar)^3} \frac{1}{\exp\left(\epsilon_p - \mu_B\right)/T + 1} \tag{6}$$

[2] The numerical tables with the distributions of the (p, π) pairs in the freeze-out temperature-density are available from the authors as data files.

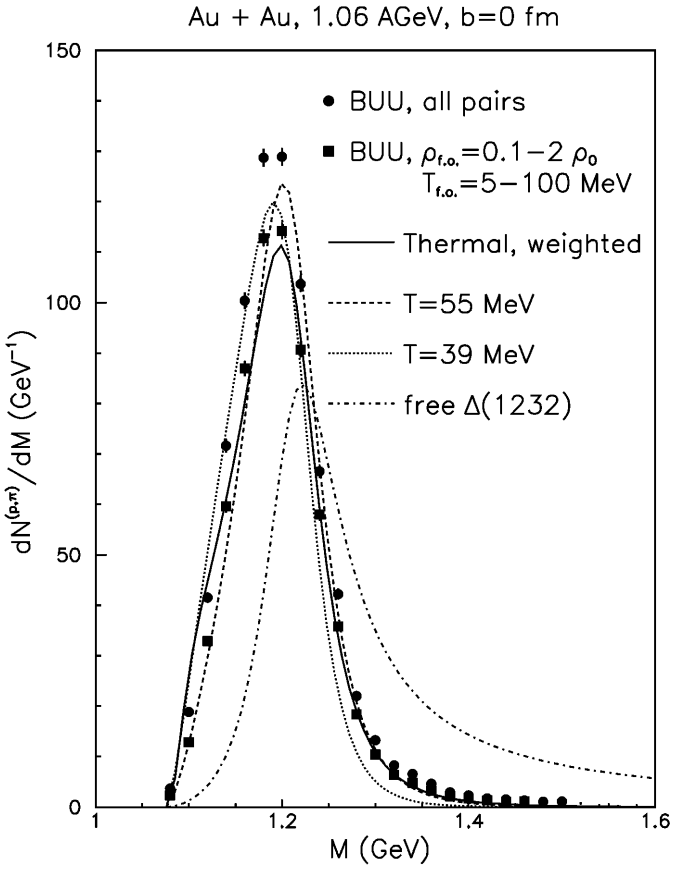

Fig. 5. (p,π) ($\pi=\pi^-,\pi^0,\pi^+$) invariant mass spectra from the BUU calculations for central Au+Au collisions at 1.06 AGeV for all pairs (filled circles) and for pairs emitted at $T_{f.o.} = 5 \div 100$ MeV and $\rho_{f.o.} = 0.1 \div 2\rho_0$ (filled squares) in comparison to the thermal model calculation at the temperature $T = 39$ MeV and the baryon density $\rho_B = 0.41\rho_0$ (dotted line), $T = 55$ MeV and $\rho_B = 0.41\rho_0$ (dashed line), and weighted with the distribution function $\partial^2 N_{pair}(T_{f.o.},\rho_{f.o.})/\partial T_{f.o.}\partial\rho_{f.o.}$ according to (8) (solid lines). The free spectral function $\mathcal{A}(M)$ (1) is shown by the dash-dotted line. Curves for fixed temperatures and the free spectral function are normalized to the number of pairs emitted at $T_{f.o.} = 5 \div 100$ MeV and $\rho_{f.o.} = 0.1 \div 2\rho_0$. No acceptance cuts were applied in selecting the pairs

with $\epsilon_p = \sqrt{M^2+p^2}$. In (6) $\mathcal{A}(M)$ is the spectral function of the Δ-resonance given by (1). The mass distribution of the Δ-resonance at finite chemical potential μ_B and temperature T is

$$\frac{dN_\Delta}{dM} = \mathcal{A}(M) 16V \int \frac{d^3p}{(2\pi\hbar)^3} \frac{1}{\exp\left(\epsilon_p - \mu_B)/T + 1\right.} \ , \quad (7)$$

where V is the freeze-out volume.

In Fig. 5 we show the invariant mass (p,π) distributions from the BUU calculations and the Δ-mass distribution (7) at various temperatures for the baryon density $\rho_B = \langle\rho_{f.o.}\rangle = 0.41\rho_0$. For comparison, the spectral function $\mathcal{A}(M)$ (1) is also shown (dot-dashed lines). The high-mass tail of the spectral function ($M \geq 1.3$ GeV) is populated very weakly. Furthermore, the resulting (p,π) invariant mass spectra have a shape quite different from the function $\mathcal{A}(M)$ due to the presence of the integral over the Fermi distribution in (7). The peak of the distribution dN_Δ/dM is slightly shifting to higher masses with increasing temperatures. We see that the BUU invariant mass spectrum is close to the thermal one for $T \simeq 40 \div 50$ MeV.

A better understanding of the BUU results is achieved if we weight the thermal model calculation with the distribution function $\partial^2 N_{pair}(T_{f.o.},\rho_{f.o.})/\partial T_{f.o.}\partial\rho_{f.o.}$ of the (p,π) pairs (Fig. 3). Then the invariant mass spectrum of the pairs reads as follows (see Appendix for a derivation):

$$\frac{dN_{pair}}{dM} = \int dT \int d\rho \frac{\partial^2 N_{pair}(T,\rho)}{\partial T \partial \rho} \cdot \frac{\Gamma(M)\frac{\partial N_\Delta(M,T,\rho)}{\partial M}}{\int\limits_{M_N+M_\pi}^{\infty} dM'\,\Gamma(M')\frac{\partial N_\Delta(M',T,\rho)}{\partial M'}} \ . \quad (8)$$

The distribution (8) is shown by solid lines in Fig. 5. In (8) we calculated the integrals for limits $T = 5 \div 100$ MeV, $\rho = 0.1 \div 2\rho_0$. In this way the pairs emitted early at non-equilibrium (high density) and late (low density) stages of the heavy-ion collision were removed from the analysis. The weighted distribution fits the BUU spectrum better than a calculation with fixed temperature and density using (7). Note that (8) has no free parameters: it only uses as an input the distribution of the emitted pairs at freeze-out temperature and density. Therefore, the mass distribution of the emitted pairs from central collisions is consistently described with a local thermal equilibrium assumption in agreement with the analysis in [7,8].

3.2 Extraction of the correlated $(p,\pi^{\pm})$ pairs by background subtraction

The experimental extraction method of the correlated $(p,\pi^{\pm})$ pairs is based on background subtraction from the event-by-event spectrum [6–8,11]. A standard way of the background construction is the event mixing technique [11]. We have, therefore, also prepared mixed BUU events taking protons and pions from different events.In the case of Au+Au collisions all events were taken at b=0 fm. For the reaction Ni+Ni we have taken events for b = 1,2 and 3 fm, and a mixed event can be composed of two events at different impact parameters[3]. We have checked that an additional restriction of equal impact parameters in both events does not influence the result in this case, since the collision dynamics changes strongly only for b≈ 5 fm. For the reaction Ni+Cu a mixing of $b = 1, 2 \ldots 5$ fm events was performed selecting event pairs with equal impact parameters only. Then the difference spectrum agrees with the spectrum of real pairs. However, for the Ni+Cu reaction, the mixing of the events without imposing any condition on the impact parameters produces a difference spectrum peaked at about 1.15 GeV, i.e. at much smaller invariant mass, since the background spectrum gets shifted to

[3] The background construction was done only for the beam energy of 1.93 AGeV in the case of Ni+Ni collisions.

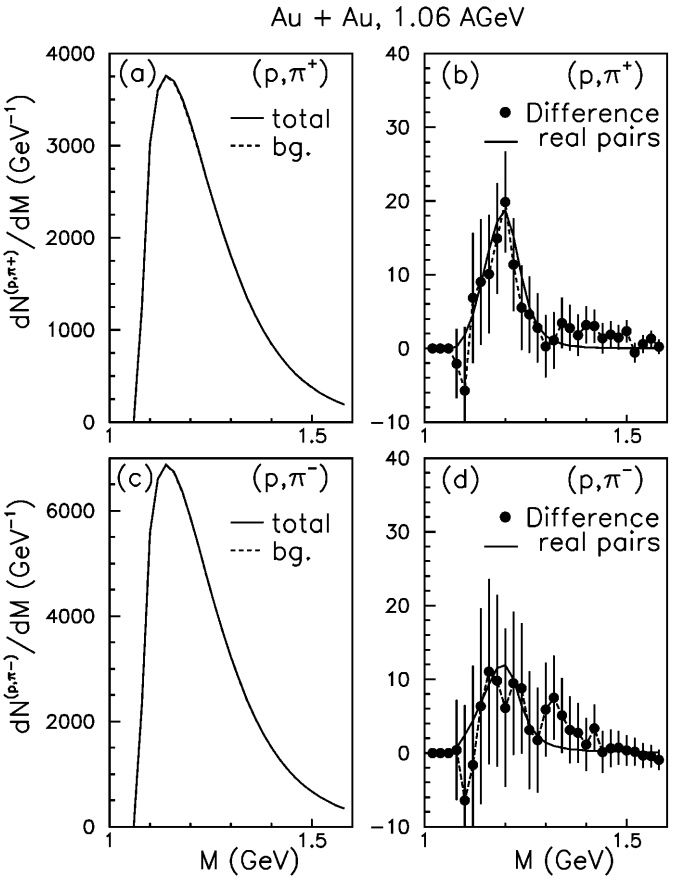

Fig. 6. The left panels show the spectra of all (p, π^+) – (a) and (p, π^-) – (c) pairs extracted event-by-event (solid line) and by event mixing (dashed line) from the BUU calculation for Au+Au at 1.06 AGeV. The right panels present the corresponding differences between event-by-event and mixed-event spectra of (p, π^+) – (b) and (p, π^-) – (d) pairs (points with errorbars connected by dashed line) and the spectra of real pairs from the same BUU calculation (solid line). The particle selection was performed including the CDC acceptance

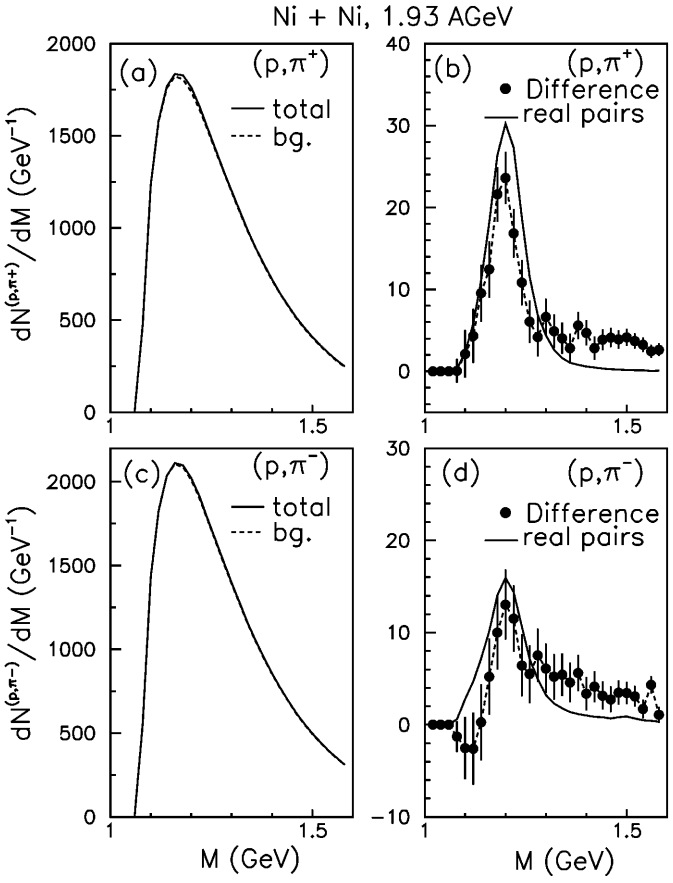

Fig. 7. The same as Fig. 6, but for Ni+Ni collisions at 1.93 AGeV

higher invariant masses. The conclusion is that the difference spectrum resembles the spectrum of real pairs only if both events selected for mixing have impact parameters within 3 fm. Note, that in our BUU study the reaction plane is fixed and, in distinction to the analysis of the experimental data in [7], we did not rotate our events around the beam axis.

In Figs. 6–8 the total event-by-event and background spectra (a,c) and their differences (b,d) are shown for the systems Au+Au, Ni+Ni and Ni+Cu. For the event mixing procedure we have prepared sets of 30000, 66000 and 24000 BUU-events for Au+Au, Ni+Ni and Ni+Cu reactions, respectively. In order to reduce the computational time, these events were calculated with the Coulomb interaction switched off (for a discussion of the Coulomb effects see the next section). The number of mixed events is 10 times more for each reaction. The real correlated pairs, selected event-by-event, were extracted in parallel from the BUU-events.

The difference spectra (points with errorbars in Figs. 6–8 (b,d)) reveal a clear correlation signal at the invariant mass $M \simeq 1.2$ GeV, in agreement with the spectra of the correlated pairs (solid lines).

The general agreement between the spectra of real $(p, \pi^{\pm})$ pairs and the difference spectra opens the possibility to identify the spectrum of real pairs given by BUU with the experimental difference spectrum. In this way one can get rid of large statistical errors, which are mostly due to the background constructed from mixed BUU events. At the same time, when doing such a comparison, we neglect some systematical deviations of the difference spectrum, which depends on the adopted background construction procedure, from the spectrum of real correlated pairs, which is unambiguous. For instance, we see from Figs. 6–8 that, in distinction to the real spectrum, the difference spectrum can show a negative correlation and an increased high invariant mass tail. Therefore, we will concentrate only on the gross structure (like the peak position and the width) of the calculated and measured spectra.

3.3 Comparison of BUU with the experimental data

In Figs. 9–11 we show the invariant mass distributions of the correlated (p, π^-) – (a) and (p, π^+) – (b) pairs

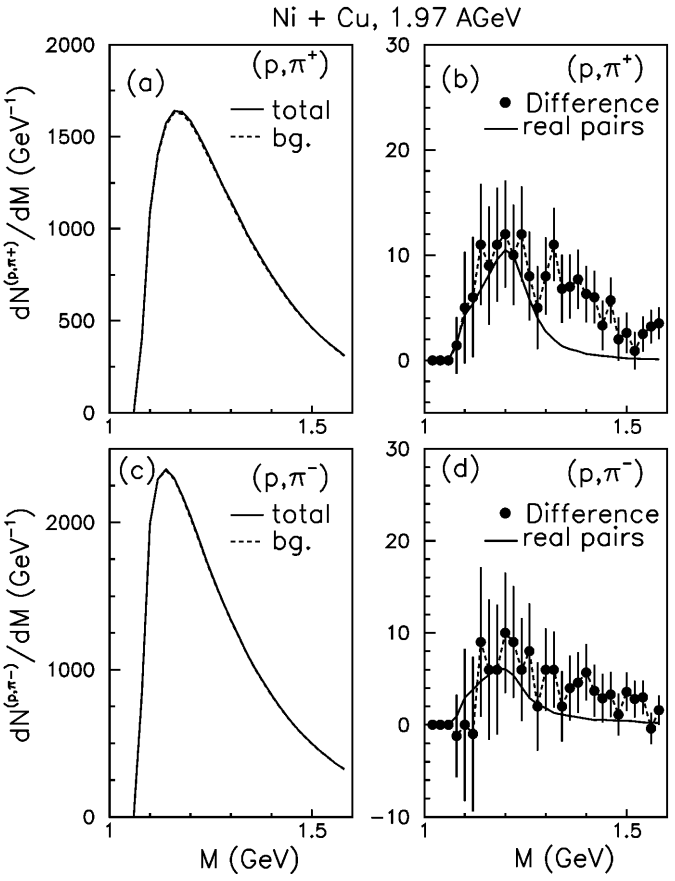

Fig. 8. The same as Fig. 6, but for Ni+Cu collisions at 1.97 AGeV. Particles are selected in full 4π acceptance. The Λ-decay contribution to the (p, π^-) spectra is dropped

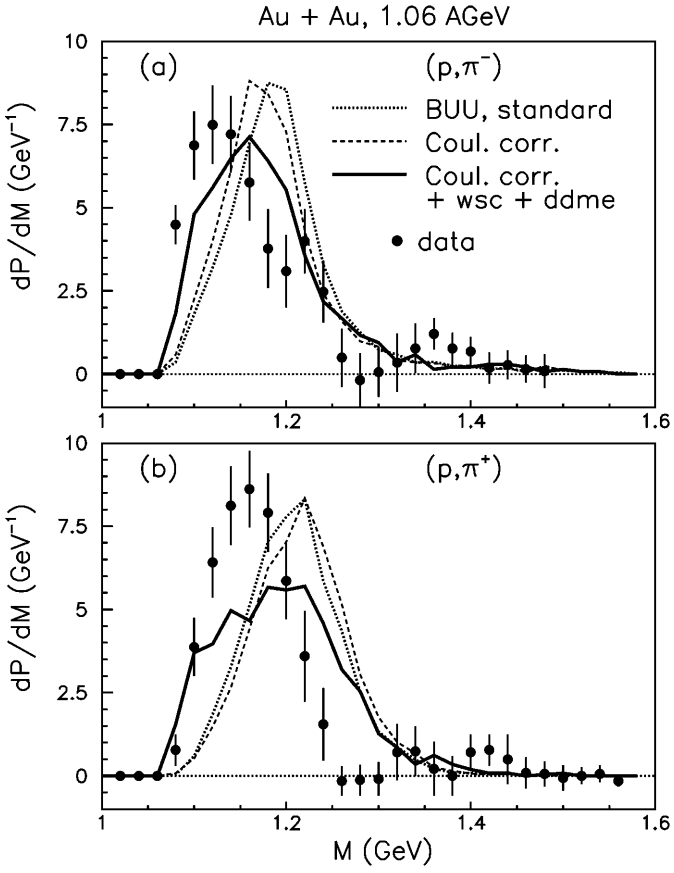

Fig. 9. Invariant mass spectra of (p, π^-) (a) and (p, π^+) (b) pairs from central Au+Au collisions at 1.06 AGeV in comparison to the data from [7]. Dotted lines – standard BUU parameterset, dashed lines – standard BUU with Coulomb final state interaction, solid lines – BUU calculation with selfconsistent width of the Δ-resonance and a density-dependent matrix element (see text for details) plus Coulomb final state interaction. All spectra are normalized to unity

for Au+Au at 1.06 AGeV (Fig. 9), Ni+Ni at 1.06 AGeV (Fig. 10) and Ni+Ni at 1.93 AGeV (Fig. 11) reactions in comparison to the experimental data of [7]. The experimental acceptance of the CDC was taken into account in our calculations. The theoretical curves are averaged over impact parameter in the range $b < 3$ fm, that approximately corresponds to the PM5 multiplicity bin (see [7]). Results with a standard parameterset of the BUU model are shown by dotted lines. These results are obtained taking into account the Coulomb interactions between charged particles in the BUU calculation. However, it was supposed in the standard calculation, that the momenta of all particles are frozen after 40 fm/c and, therefore, the residual Coulomb energy was neglected. The effect of the residual Coulomb energy was, furthermore, taken into account by rescaling the momenta of particles as:

$$\mathbf{p} \to \kappa \mathbf{p}, \qquad \kappa = (2mU_{coul}/p^2 + 1)^{1/2} \ , \qquad (9)$$

where U_{coul} is the Coulomb energy of a particle at $t = 40$ fm/c. The residual Coulomb energy shifts the spectra of (p, π^-) and (p, π^+) pairs to smaller and larger invariant masses, respectively, by about $5 \div 10$ MeV (dashed lines).

The complete role of the Coulomb interactions can be seen now, e.g. from a comparison of the solid line in Fig. 6d with the dashed line in Fig. 9a. We see that the Coulomb effects are shifting the peak of the (p, π^-) spectrum in the Au+Au central collisions by about -50 MeV. The corresponding shift of the (p, π^+) spectrum is about +20 MeV for the same reaction. At higher beam energies of about 2 AGeV the role of the Coulomb interactions becomes negligible for the Ni+Ni and Ni+Cu systems.

We have also performed a calculation considering the width of the Δ-resonance selfconsistently, i.e. taking into account the Pauli blocking of the decay $\Delta \to N\pi$, the absorption $\Delta N \to NN$ and the rescattering $\Delta N \to \Delta N$. This dynamical width of the Δ-resonance then has been used in (1) for the spectral function (see [17] for details). Moreover, since quite high central densities $\sim 2.5\rho_0$ are reached in central heavy-ion collisions at $1 \div 2$ AGeV, a medium modification of the matrix element for the process $\Delta N \to NN$ simulating the effect of a direct three-body absorption (see also [12]) was included as follows:

$$|\mathcal{M}_{\Delta N \to NN}|^2 = \left(1 + 3\frac{\rho}{\rho_0}\right) |\mathcal{M}^{vac}_{\Delta N \to NN}|^2 \ . \qquad (10)$$

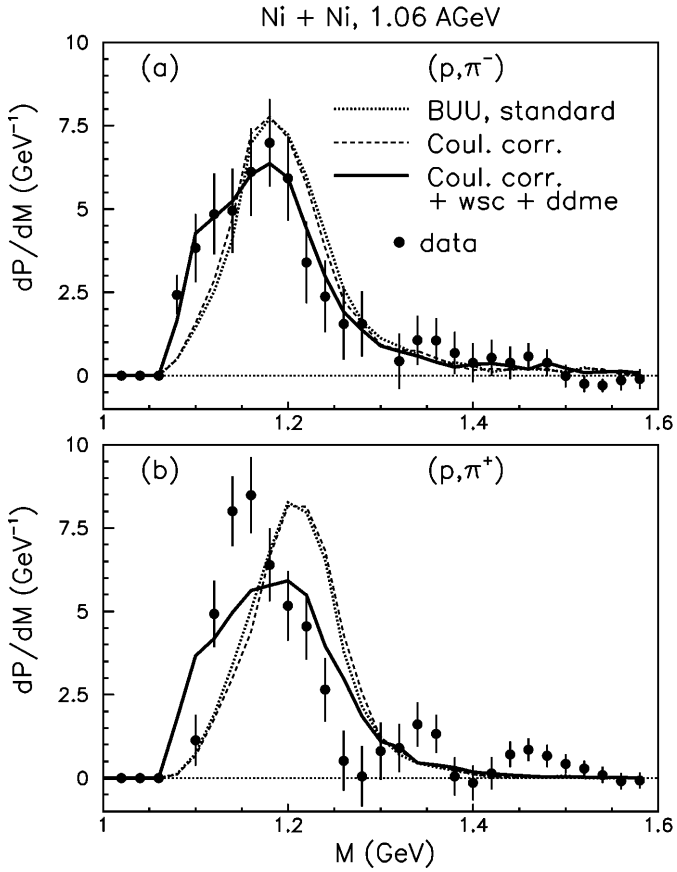

Fig. 10. The same as Fig. 9, but for central collisions of Ni+Ni at 1.06 AGeV

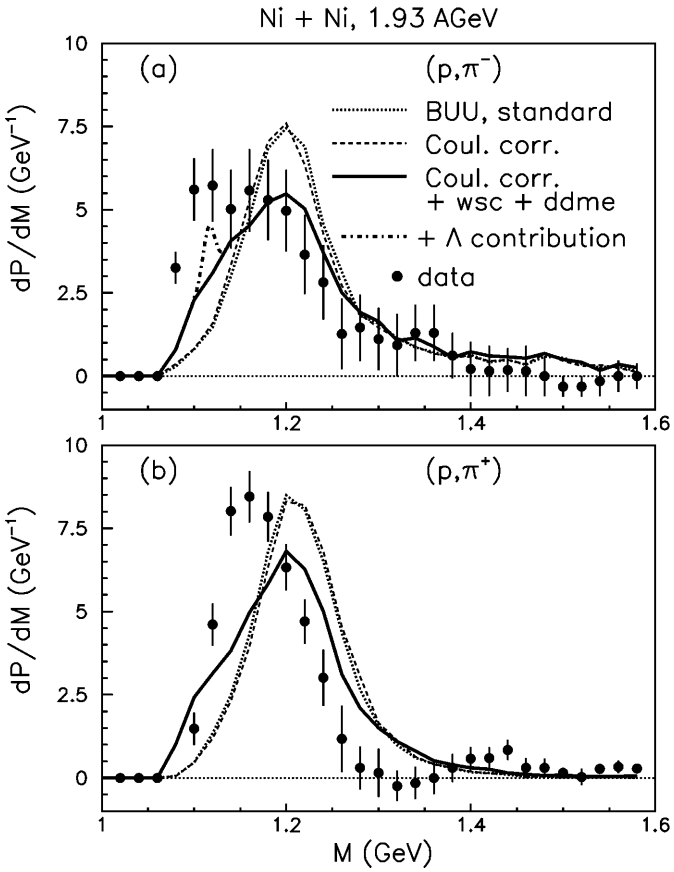

Fig. 11. The same as Fig. 9, but for central collisions of Ni+Ni at 1.93 AGeV. The dot-dashed line shows the Λ decay contribution to the spectrum of (p, π^-) pairs added to the Δ^0 decay spectrum calculated with selfconsistent width of the Δ-resonance and density-dependent matrix element

The solid lines in Figs. 9–11 show the calculations including the selfconsistent Δ-width (wsc) and the density-dependent matrix element (ddme) of (10). It gives essentially broader invariant mass spectra and shifts the peaks to smaller invariant masses, however, still not enough to explain the FOPI data on (p, π^+) pairs.

One observes, nevertheless, a rather good overall agreement of the wsc+ddme calculation to the FOPI data on (p, π^-). For the Ni+Ni collisions at 1.93 AGeV (Fig. 11a), the (p, π^-) data reveal a double-humped structure with an additional peak at low invariant mass, which can be explained by the decay $\Lambda \to p\pi^-$ (c.f. [6]). This decay creates a narrow peak at the invariant mass of 1.116 GeV. We obtained on average $\simeq 0.1$ (p, π^-) pairs per event in central collisions of Ni+Ni at 1.93 AGeV and of Ni+Cu at 1.97 AGeV (see below) due to the Λ decays. The channels $NN \to \Lambda KN$ and $NN \to \Sigma^0 KN$ followed by $\Sigma^0 \to \Lambda\gamma$ were taken into account in the calculation of the Λ production. The Λ contribution to the (p, π^-) spectrum is shown by the dot-dashed line on top of the wsc+ddme curve in Fig. 11a. This contribution was parameterized by a gaussian of width $\sigma = 6.4$ MeV/c^2 determined by the bin size 20 MeV/c^2 of the calculated spectrum.

Figures 12, 13 show the results for the Ni+Cu reaction at 1.97 AGeV in comparison to the data from [6]. For this reaction we have performed only the wsc+ddme calculation. The calculated results are not filtered through the EOS-TPC acceptance. Again, we can observe, however, a good agreement with the (p, π^-) data taking into account the Λ decay. We note, that the relative Λ contribution is larger in the Ni+Cu reaction than in the very similar Ni+Ni reaction. This is caused by the $5 \div 6$ times reduction of the number of (p, π^-) pairs due to the Λ decays after filtering through the CDC acceptance, while the number of $(p, \pi^{\pm})$ pairs produced by the Δ decays gets reduced only by a factor of $3 \div 4$ (see Table 2). We attribute this different reduction to a smaller directed Λ flow than proton flow (c.f. [18]). For (p, π^+) pairs (Figs. 12b and 13), the calculations still overpredict the peak position of the Δ^{++} by about 10 MeV, but the overall agreement with the EOS-TPC data on (p, π^+) pairs is better than for the FOPI data.

It was shown in [6], that the peak of the (p, π^+) invariant mass distribution shifts to lower invariant masses with the centrality of the collision. Figure 13 shows, that also in the BUU calculations the same effect is present since in peripheral nucleus-nucleus collisions the emitted proton-pion pairs are mostly due to decays of Δ-resonances excited in energetic first-chance nucleon-nucleon collisions,

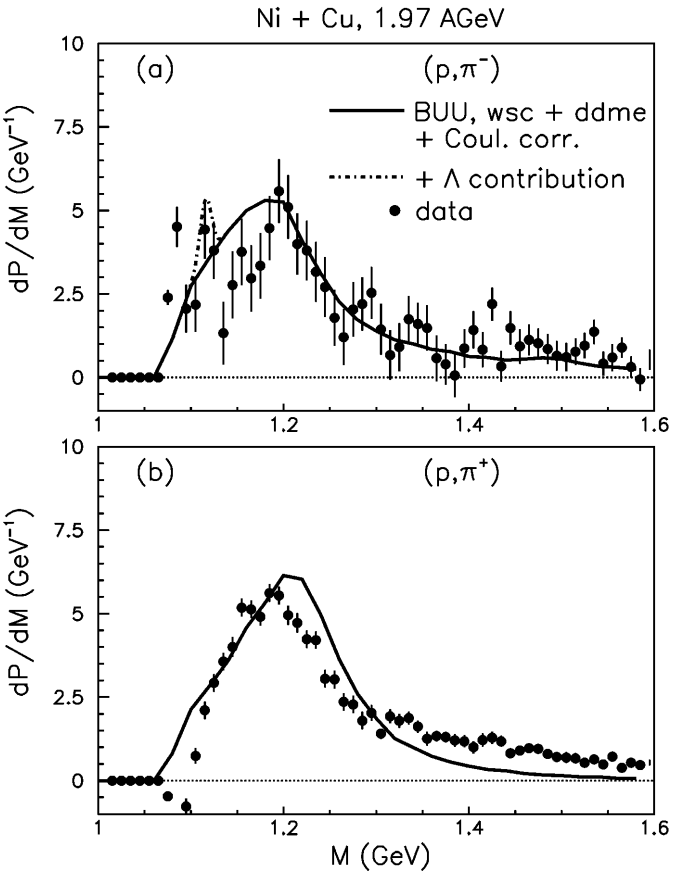

Fig. 12. The same as Fig. 9, but for Ni+Cu collisions at 1.97 AGeV. The BUU calculation is performed with selfconsistent Δ-width and density-dependent matrix element for the impact parameter region b=$0 \div 10$ fm. The final state Coulomb interaction is taken into account. The Λ decay contribution to the spectrum of (p,π^-) pairs added to the Δ^0 decay spectrum is shown by the dot-dashed line. The experimental data are from [6]

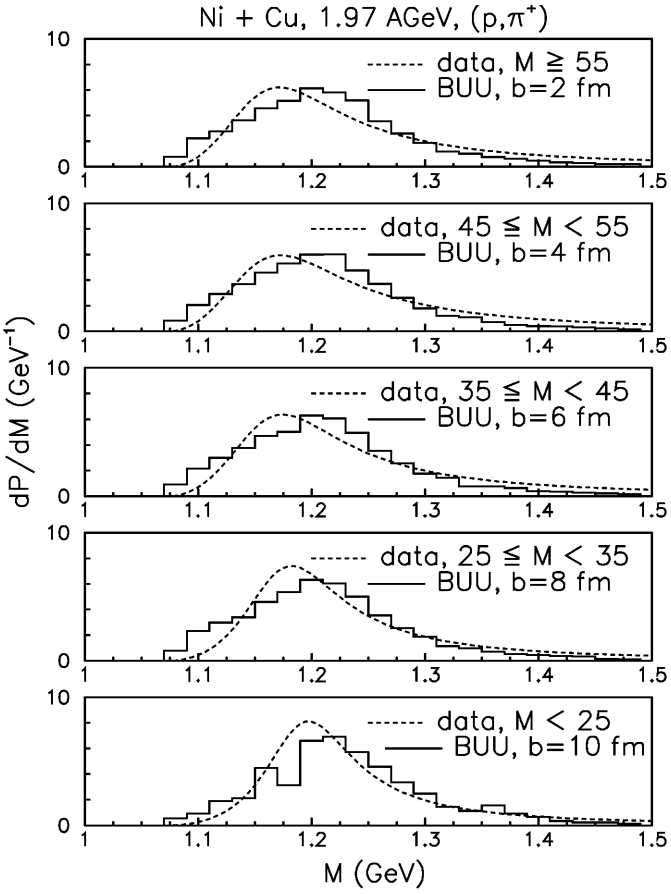

Fig. 13. Invariant mass spectra of (p,π^+) pairs for Ni+Cu collisions at 1.97 AGeV at different centrality. The BUU calculations (performed with selfconsistent Δ-width and density-dependent matrix element) are presented by histograms for b=2,4,6,8 and 10 fm from the uppermost to lowermost panel. The Breit-Wigner fits to the data from [6] are shown by dashed lines for the multiplicities $M \geq 55$, $45 \leq M < 55$, $35 \leq M < 45$, $25 \leq M < 35$ and $M < 25$. The spectra are normalized to unity

where the thermal picture discussed in Sect. 3.1 does not apply. We should remark that our statistics is rather poor for peripheral collisions. Therefore, the discussed shift in our calculations in Fig. 13 is more relevant for the average value of the distribution than for the peak position.

3.4 Comparison of the BUU+thermal calculations to the experimental data

We have studied the predictions of the thermal model using as an input the distribution of (p,π) pairs at the freeze-out temperature and density produced by BUU (8). This hybrid approach offers an easy possibility to see the influence of the spectral function in the thermal part of the calculation on the observed Δ-mass spectrum while *retaining in BUU the bare spectral function* $\mathcal{A}$ (1). Besides the calculations with the bare spectral function $\mathcal{A}$ in the thermal part, we have performed a thermal model analysis replacing $\mathcal{A}$ in (6),(7) by the derivative of the πN-scattering phase shift in the P_{33} channel with respect to the center-of-mass energy of the pion and nucleon ([5]):

$$\mathcal{B}(E_{cm}) = 2\frac{\partial \delta_{33}(E_{cm})}{\partial E_{cm}}. \qquad (11)$$

The $\mathcal{B}$-function (11) can be interpreted as a level density of the πN system (cf. [19] and Refs. therein). The thermal model employing the $\mathcal{B}$-function (11) gives a better agreement with the experimental π^0 transverse mass spectrum for the Au+Au reaction at 1 AGeV as shown in [5]. To clarify the reason we compare in Fig. 14 the spectral function $\mathcal{A}$ (solid line) with the weight function $\mathcal{B}/2\pi$ (dashed line) (see also Fig. 2 in [5]). The $\mathcal{B}$-function yields an increased contribution at smaller invariant masses.

Figure 15 demonstrates the results of the hybrid BUU+thermal calculations based on (8) for various systems in comparison to the data from [6,7]. For this comparison, we have selected the data on (p,π^+), since: (i) the statistics for (p,π^+) is always better than for (p,π^-),

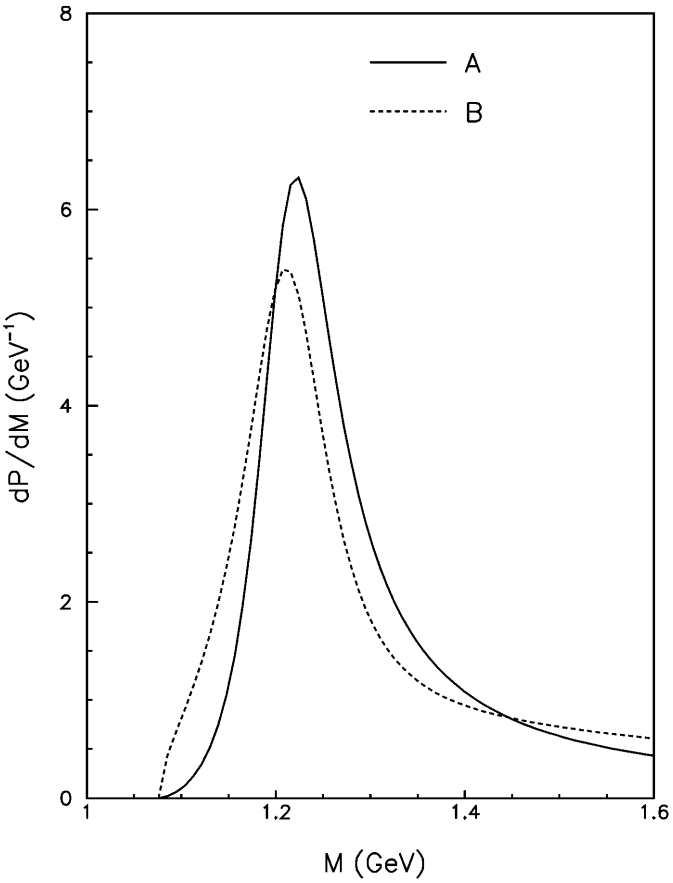

Fig. 14. The spectral function $\mathcal{A}$ of the free Δ (solid line) and the weight function $\mathcal{B}/2\pi$ (dashed line) versus invariant mass

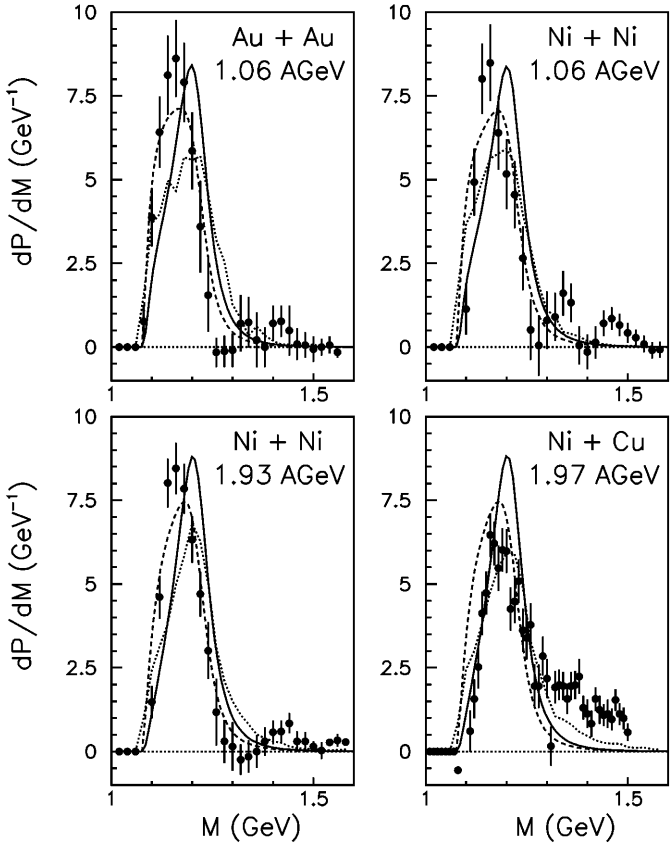

Fig. 15. Thermal invariant mass distributions using functions $\mathcal{A}$ (solid lines) and $\mathcal{B}$ (dashed lines) weighted according to (8) in comparison to the data on (p, π^{+}) pairs from [7] (Au+Au and Ni+Ni central collisions) and from [6] (Ni+Cu collisions with multiplicity $M \geq 55$). The dotted lines show the BUU (wsc+ddme) results for central collisions. All curves are normalized to unity

and (ii) the (p, π^{+}) signal from the Δ^{++} is not contaminated by the decays of higher baryon resonances and by the Λ decay. The solid lines in Fig. 15 show the BUU + thermal calculation with the $\mathcal{A}$-function. This calculation strongly overpredicts the peak positions in the case of Au+Au and Ni+Ni reactions (see also dotted lines obtained within the BUU only in Figs. 9–11 b). The agreement is somewhat better in the case of the Ni+Cu reaction. For the $\mathcal{B}$-function (dashed lines), the peak of the theoretical spectrum of the pairs shifts to smaller invariant masses while the width increases. Thus, the agreement of the thermal calculation with the FOPI data is improved by the $\mathcal{B}$-function. The residual discrepancies can be further diminished by accounting for the Coulomb effects in the calculations (c.f. [7]). However, the $\mathcal{B}$-function leads to a worse agreement for the Ni+Cu reaction, which can be explained reasonably well only within the BUU (wsc+ddme) calculation (dotted lines in Fig. 15). This calculation, however, is still not consistent with the FOPI data on (p, π^{+}).

4 Summary and conclusions

In this work a study of correlated $(p, \pi^{\pm})$ pair emission from central heavy-ion collisions at energies of $1 \div 2$ AGeV has been performed within the BUU transport model. In agreement with the data [7] less than 1% of the total number of the $(p, \pi^{\pm})$ pairs are correlated. Our calculations give $\approx 25\%$ of emitted pions in correlations with protons (the rest of pions are produced either directly or their correlations are destroyed by proton and/or pion rescattering) for Au+Au central collisions at 1.06 AGeV. This value is lower than the one reported in [7] of $\geq 50\%$ of pions correlated with protons. Since the total pion multiplicity is also overpredicted by the BUU model for the Au+Au reaction by about a factor of 1.7, the number of correlated pairs per event turns out to be close to the data again.

The correlated pairs originate from Δ-decays in low-density regions during an intermediate stage ($t = 20 \div 30$ fm/c) of the collision. The calculated invariant mass spectra of these pairs have a thermal shape; however, the real (kinetic) temperature in the system changes quite strongly during the period of emission. This result is related to a weak sensitivity of the shape of the invariant mass spectra to the temperature in the region $T = 40 \div 55$ MeV, which follows from a simple thermodynamical calculation (see text and Fig. 5). We would like to stress, that *the*

freeze-out of the pairs happens during an extended period of time, comparable with the time scale of the heavy-ion collision itself. Therefore, the thermodynamical state of the system is changing quite strongly during this period.

The BUU calculation with the selfconsistent treatment of the Δ-width and the medium-modified matrix element for the process $N\Delta \to NN$ (see Sect. 3.3) gives a good overall agreement with both the FOPI and EOS-TPC data on the (p, π^-) invariant mass distributions. The calculated (p, π^+) spectra are shifted to higher invariant masses with respect to the FOPI data, but are in reasonable agreement with the EOS-TPC data. It is, therefore, an open question if some additional effects influencing the Δ propagation and decay in hot and dense nuclear matter are needed to account for the remaining shift in future dynamical calculations. In particular, the approach taking into account the vacuum πN scattering phase shift [5,20] gives a better agreement with the FOPI data, as demonstrated within the thermodynamical model in [7] and in Sect. 3.4 of the present work; however, it gives a worse description of the EOS data from the BEVALAC. This conflicting situation calls for new experiments on (p, π) correlations.

We are grateful to E.L. Bratkovskaya, C. Greiner and A.A. Sibirtsev for helpful discussions and their interest in this work. Furthermore, the authors would like to thank D. Pelte for a careful reading of the manuscript and helpful advice.

Appendix

In this Appendix we derive (8) for the mass distribution of emitted pairs.

The density of emitted pairs in the space invariant mass – freeze-out temperature – freeze-out density is (for brevity we drop lower indices at $T_{f.o.}$ and $\rho_{f.o.}$):

$$\frac{\partial^3 N_{pair}(M,T,\rho)}{\partial M \partial T \partial \rho} = W\Gamma(M) \cdot \int_0^\infty dt \, \frac{\partial^3 N_\Delta(M,T,\rho,t)}{\partial M \partial T \partial \rho} \ , \quad (12)$$

where $\frac{\partial^3 N_\Delta(M,T,\rho,t)}{\partial M \partial T \partial \rho}$ is the density of Δ-resonances in the same space as a function of time, $\Gamma(M)$ is the decay width of (2), and W is the surviving probability of an emitted pair assumed to be independent on invariant mass, temperature and density. We have:

$$\frac{\partial^2 N_{pair}(T,\rho)}{\partial T \partial \rho} = \int_{M_N+M_\pi}^\infty dM \, W\Gamma(M) \cdot \int_0^\infty dt \, \frac{\partial^3 N_\Delta(M,T,\rho,t)}{\partial M \partial T \partial \rho} \ . \quad (13)$$

Assuming local thermal equilibrium we can write:

$$\frac{\partial^3 N_\Delta(M,T,\rho,t)}{\partial M \partial T \partial \rho} = \frac{\partial^2 N_\Delta(T,\rho,t)}{\partial T \partial \rho} \frac{\partial \tilde{N}_\Delta(M,T,\rho)}{\partial M} \ , \quad (14)$$

where

$$\frac{\partial \tilde{N}_\Delta(M,T,\rho)}{\partial M} = \frac{\partial N_\Delta(M,T,\rho)}{\partial M} \cdot \left[\int_{M_N+M_\pi}^\infty dM' \, \frac{\partial N_\Delta(M',T,\rho)}{\partial M'} \right]^{-1} \quad (15)$$

is the mass distribution of Δ-resonances (see (7)) normalized to 1, which depends only on the local temperature and density.

Substituting (14),(15) into (12) and (13), we obtain the expressions:

$$\frac{\partial^3 N_{pair}(M,T,\rho)}{\partial M \partial T \partial \rho} = \xi_\Delta(\rho,T) W\Gamma(M) \frac{\partial \tilde{N}_\Delta(M,T,\rho)}{\partial M} \quad (16)$$

$$\frac{\partial^2 N_{pair}(T,\rho)}{\partial T \partial \rho} = \xi_\Delta(\rho,T) \cdot \int_{M_N+M_\pi}^\infty dM \, W\Gamma(M) \frac{\partial \tilde{N}_\Delta(M,T,\rho)}{\partial M} \quad (17)$$

with

$$\xi_\Delta(\rho,T) = \int_0^\infty dt \, \frac{\partial^2 N_\Delta(T,\rho,t)}{\partial T \partial \rho} \ . \quad (18)$$

Using (16),(17) and the relation

$$\frac{dN_{pair}}{dM} = \int dT \int d\rho \, \frac{\partial^3 N_{pair}(M,T,\rho)}{\partial M \partial T \partial \rho} \quad (19)$$

it is straightforward to obtain (8).

References

1. W. Ehehalt, W. Cassing, A. Engel, U. Mosel, and Gy. Wolf, Phys. Rev. C **47**, R2467 (1993)
2. S.A. Bass, C. Hartnack, H. Stöcker, and W. Greiner, Phys. Rev. C **51**, 3343 (1995)
3. C.M. Ko and G.Q. Li, J. Phys. G **22**, 1673 (1996)
4. S. Teis, W. Cassing, M. Effenberger, A. Hombach, U. Mosel and Gy. Wolf, Z. Phys. A **356**, 421 (1997)
5. W. Weinhold, B. Friman and W. Nörenberg, Phys. Lett. B **433**, 236 (1998); nucl-th/9710014
6. E.L. Hjort et al., Phys. Rev. Lett. **79**, 4345 (1997)
7. M. Eskef, D. Pelte, FOPI collaboration, Eur. Phys. J. A **3**, 335 (1998)
8. D. Pelte, nucl-ex/9902006
9. W. Cassing, V. Metag, U. Mosel and K. Niita, Phys. Rep. **188**, 363 (1990); W. Cassing and E.L. Bratkovskaya, Phys. Rep. **308**, 65 (1999)

10. M. Effenberger, E.L. Bratkovskaya, and U. Mosel, Phys. Rev. C **60**, 044614 (1999)
11. D. L'Hôte, Nucl. Instr. and Meth. A **337**, 544 (1994)
12. A. Engel, W. Cassing, U. Mosel, M. Schäfer and Gy. Wolf, Nucl. Phys. A **572**, 657 (1994)
13. M. Effenberger, A. Hombach, S. Teis, U. Mosel, Nucl. Phys. A **613**, 353 (1997)
14. **FOPI** Collaboration: D. Pelte et al., Z. Phys. A **357**, 215 (1997)
15. A. Hombach, W. Cassing, S. Teis and U. Mosel, Eur. Phys. Jour. A **5**, 157 (1999)
16. J. Cleymans, H. Oeschler and K. Redlich, J. Phys. G **25**, 281 (1999)
17. M. Effenberger, A. Hombach, S. Teis and U. Mosel, Nucl. Phys. A **614**, 501 (1997)
18. G.Q. Li and C.M. Ko, Phys. Rev. C **54**, 1897 (1996)
19. J. Knoll, Prog. Part. Nucl. Phys. **42**, 177 (1999)
20. P. Danielewicz and S. Pratt, Phys. Rev. C **53**, 249 (1996)